OCEAN OXYGEN

Oxygen rise in the tropical upper ocean during the Paleocene-Eocene Thermal Maximum

Simone Moretti[1,2]*, Alexandra Auderset[1,3], Curtis Deutsch[4], Ronja Schmitz[1], Lukas Gerber[1], Ellen Thomas[5,6], Valeria Luciani[7], Maria Rose Petrizzo[8], Ralf Schiebel[1], Aradhna Tripati[9,10,11], Philip Sexton[12], Richard Norris[13], Roberta D'Onofrio[7]†, James Zachos[14], Daniel M. Sigman[4], Gerald H. Haug[1], Alfredo Martínez-García[1]*

The global ocean's oxygen inventory is declining in response to global warming, but the future of the low-oxygen tropics is uncertain. We report new evidence for tropical oxygenation during the Paleocene-Eocene Thermal Maximum (PETM), a warming event that serves as a geologic analog to anthropogenic warming. Foraminifera-bound nitrogen isotopes indicate that the tropical North Pacific oxygen-deficient zone contracted during the PETM. A concomitant increase in foraminifera size implies that oxygen availability rose in the shallow subsurface throughout the tropical North Pacific. These changes are consistent with ocean model simulations of warming, in which a decline in biological productivity allows tropical subsurface oxygen to rise even as global ocean oxygen declines. The tropical oxygen increase may have helped avoid a mass extinction during the PETM.

Oxygen is fundamental to life, and its distribution in the ocean constrains the habitats of marine biota, from microbes to macrofauna. Historical observations demonstrate a strong correlation between the rise in ocean heat content and declining oxygen inventory over the past five decades (*1*, *2*), with substantial impacts on coastal ecosystems (*3*, *4*). Although these global trends are likely to persist into the future (*5*), their regional manifestations are poorly understood, particularly in the tropical ocean, which contains some of the greatest biodiversity, most productive ecosystems, and lowest oxygen concentrations in the global ocean (*6*–*8*). Nitrogen isotope measurements in sedimentary archives from the vicinity of the oxygen-deficient zones (ODZs) provide a window into ODZ response to climate change. Reconstructions from the past century suggest that the ODZ in the eastern tropical North Pacific, the largest ODZ of the global ocean, shrinks when trade winds weaken, a trend that is anticipated from climate warming (*6*). Contraction of the North Pacific ODZ has also been inferred during peak warmth in the Eocene and Miocene epochs (*9*, *10*). However, the prominence of centennial variability in signals from the recent past (*6*) and the potential importance of geological processes in records spanning millions of years (*11*) leave doubt about the relevance of these changes for the ODZs under anthropogenic warming. Moreover, the colder climate of the Last Glacial Maximum ~20,000 years ago may have also had smaller ODZs (*12*), which is the opposite sensitivity of ODZs to climate implied by the Eocene and Miocene data, although this result has recently been questioned (*13*). Thus, the fate of the ODZs in warming climates and their connection to the broader oxygen conditions of the tropical ocean remain uncertain.

The Paleocene-Eocene Thermal Maximum (PETM) was the largest and fastest known pre-anthropogenic global warming event in the Cenozoic (*14*). It occurred around 56 million years ago in response to a rapid (<5000 year) (*15*) injection of carbon into the ocean-atmosphere system. This caused a decline in the carbon-13–to–carbon-12 ratio ($\delta^{13}C$) of preserved materials in both marine and terrestrial sedimentary archives, known as the C isotope excursion (CIE), close to the onset of the PETM (*16*). Global average temperature rose by at least 5°C (*17*), whereas atmospheric CO_2 is believed to have more than doubled (*18*). The PETM was associated with widespread ocean acidification (*19*), large faunal turnover on land (*16*), and the largest extinction of marine benthic organisms of the Cenozoic (*20*). Although the C emission was ~10 times slower than that at present (*21*), the amplitude of the reconstructed relative temperature increase resembles future climate projections under scenarios of high greenhouse gas emissions (*17*). Thus, the PETM may foreshadow the future state of ocean oxygenation. However, the response of the ODZs during this episode of abrupt warming remains highly uncertain (*22*, *23*). In this work, we reconstructed changes in the ODZs and surrounding shallow subsurface waters of the tropical ocean during the PETM using foraminifera-bound nitrogen isotopes and microfossil body size.

The stable isotopes of nitrogen have been used to study past changes in the ODZs (*12*, *24*). Denitrification that occurs in the ODZs expresses a large isotopic discrimination due to incomplete nitrate (NO_3^-) reduction in the water column, which causes residual nitrate to be enriched in ^{15}N (*25*). Circulation as well as assimilation, sinking, and regeneration propagate the ^{15}N-enriched nitrate signal of the ODZs well beyond their spatial extent (*26*), ultimately elevating nitrate $\delta^{15}N$ {$\delta^{15}N = [(^{15}N/^{14}N)_{sample}/(^{15}N/^{14}N)_{atmN2} - 1)] \times 1000‰$} throughout the Pacific and the global ocean. By contrast, sedimentary denitrification (SD) consumes N with only weak isotopic discrimination, owing to nearly complete nitrate consumption in sediment porewaters (*27*). Accordingly, mean ocean pycnocline nitrate $\delta^{15}N$ is largely controlled by the global ratio of water column denitrification (WCD) to SD (*28*). Planktic foraminifera provide a window into past seawater nitrate $\delta^{15}N$. In oligotrophic regions where surface nutrients are fully consumed, the $\delta^{15}N$ of foraminifera-bound organic matter (FB-$\delta^{15}N$) reflects the $\delta^{15}N$ of the pycnocline nitrate (*29*). Foraminifera-bound organic matter is well protected from alteration by the biomineral matrix (*30*) and has been used to reconstruct changes in the N cycle over the Cenozoic, the past 66 million years (*9*–*11*).

We report measurements of FB-$\delta^{15}N$ from five well-studied PETM sections (Fig. 1 and table S1). We present measurements of the three dominant planktic foraminifera genera of the PETM—*Subbotina*, *Acarinina*, and *Morozovella*—measured in parallel whenever their abundances allowed. We report FB-$\delta^{15}N$ data from subtropical Atlantic Ocean Drilling Program (ODP) Site 1263, Southern Ocean ODP Site 690, tropical North Pacific ODP Sites 1209 and 1210, equatorial Site 865, and Indian Ocean Deep Sea Drilling Project (DSDP) Site 213 (Fig. 1). At the paleolocations of Sites 213, 1209, 1210, and 1263, nutrient consumption in the surface waters is expected to have been complete, such that these FB-$\delta^{15}N$ data should record changes in the $\delta^{15}N$ of the nitrate in the shallow subsurface (*29*). The Pacific hosts most of the ocean's WCD along its eastern tropical margin (*31*), and Sites 1209 and 1210 were paleolocated at the margin of the eastern tropical North Pacific ODZ (Fig. 1), to which the westward transport of the denitrification N isotopic signal is well documented (*26*). This makes Sites 1209 and 1210 particularly sensitive to denitrification in the

[1]Climate Geochemistry Department, Max Planck Institute for Chemistry, Mainz, Germany. [2]Istituto di Scienze Polari, Consiglio Nazionale delle Ricerche, Bologna, Italy. [3]School of Ocean and Earth Science, University of Southampton, Southampton, UK. [4]Department of Geosciences, Princeton University, Princeton, NJ, USA. [5]Department of Earth and Planetary Sciences, Yale University, New Haven, CT, USA. [6]Department of Earth and Environmental Sciences, Wesleyan University, Middletown, CT, USA. [7]Dipartimento di Fisica e Scienze della Terra, Università di Ferrara, Ferrara, Italy. [8]Dipartimento di Scienze della Terra "Ardito Desio," Università Degli Studi di Milano, Milan, Italy. [9]Department of Earth, Planetary, and Space Sciences, University of California, Los Angeles, Los Angeles, CA, USA. [10]Department of Atmospheric and Oceanic Sciences, University of California, Los Angeles, Los Angeles, CA, USA. [11]Department of Institute of the Environment and Sustainability, University of California, Los Angeles, Los Angeles, CA, USA. [12]School of Environment, Earth and Ecosystem Sciences, The Open University, Milton Keynes, UK. [13]Scripps Institute of Oceanography, University of California, San Diego, La Jolla, CA, USA. [14]Department of Earth and Planetary Sciences, University of California, Santa Cruz, Santa Cruz, CA, USA.
*Corresponding author. Email: simone.moretti@mpic.de (S.M.); a.martinez-garcia@mpic.de (A.M.-G.)
†Present address: CNR, Marine Science Institute (ISMAR), Arsenale Castello 2737/f, 30122 Venezia, Italy.

North Pacific ODZ. By contrast, there is no WCD in the modern South Atlantic, which is the region of Site 1263, and Indian Site 213 is remote from the Arabian Sea ODZ and its denitrification signal.

ODZs during the PETM

At the onset of the PETM, FB-$\delta^{15}N$ declined at the tropical Sites in the North Pacific (Sites 1209 and 1210), South Atlantic (Site 1263), and Indian Ocean (Site 213), as well as at Site 690 in the Southern Ocean (Fig. 2, A and B; Site 865 will be discussed below). We observed the largest decline in FB-$\delta^{15}N$ in North Pacific Sites 1209 and 1210, which show an extreme FB-$\delta^{15}N$ drop from 16 per mill (‰) to 4‰ (Fig. 2A and figs. S3 to S5). This results in a collapse in the reconstructed FB-$\delta^{15}N$ difference between the Pacific and the Atlantic and Indian basins (fig. S6), before gradually recovering to pre-PETM values in parallel with foraminiferal carbonate $\delta^{13}C$ (Fig. 2D). Our FB-$\delta^{15}N$ data for the pre- and post-PETM interval are consistent with background Paleocene FB-$\delta^{15}N$ values (*9*). Importantly, at Sites 1209 and 1210, FB-$\delta^{15}N$ declines to near its lowest value without a transition through intermediate values, and this occurs within 3 cm of sediment thickness (fig. S3), pointing to a geologically instantaneous environmental change.

The observation of a FB-$\delta^{15}N$ decline at multiple sites from the different ocean basins implies a decrease in mean ocean pycnocline nitrate $\delta^{15}N$. Because the mean ocean pycnocline nitrate $\delta^{15}N$ is driven by the relative proportions of WCD and SD (*28*), our results could, in principle, be explained by either a decline in WCD or an increase in SD. However, a global increase in SD is expected to have the same isotopic impact across basins (*28*). By contrast, there is a much greater FB-$\delta^{15}N$ decline in the Pacific, as reflected in the collapse of the Pacific-to-Atlantic and Pacific-to-Indian FB-$\delta^{15}N$ gradients (Fig. 2A and fig. S6). This points to a marked decline in North Pacific WCD. Other possible changes, such as in SD and/or N fixation, may have occurred, but they cannot themselves explain the observed FB-$\delta^{15}N$ changes [see supplementary materials (SM)].

Among all our sites, Sites 1263 and 213 together likely provide the best measure of the PETM decline in mean ocean pycnocline nitrate $\delta^{15}N$ (*32*), suggesting that it was ~5‰ (Fig. 2A). A simple mass balance of the ocean N budget suggests that this corresponds to a 13 to 21% decline in the proportion of denitrification occurring in the water column (Fig. 3B and table S2). Today, North Pacific WCD accounts for ~8% of the total denitrification (*31*). Thus, the apparent whole pycnocline nitrate $\delta^{15}N$ decline of ~5‰ may require that WCD also decreased in the ocean's other ODZs.

Foraminifera size and ocean oxygen

To evaluate whether the decline in WCD implied by FB-$\delta^{15}N$ measurements reflects changes specific to the ODZs or broader changes in low-latitude oxygenation, we estimated changes in seawater P_{O_2} (partial pressure of diatomic oxygen) using foraminifera shell size (FS-P_{O_2}). Marine ectotherm species in warm waters grow to smaller body sizes when temperatures rise, a relationship that is observed experimentally and in natural environments (*33*). The magnitude of this temperature size effect (TSE) and its patterns of variability across species and a wide range of temperature and body sizes can be predicted from a mechanistic model of organism O_2 supply and demand (*34*). A rise in temperature increases metabolic O_2 demand relative to organismal O_2 supply; balance can be restored by a reduction in body size. Changes in ambient P_{O_2} induce an analogous oxygen size effect (OSE) that is also observed in aquatic species (*35*, *36*) and that may exacerbate or ameliorate the TSE. The combined impact on body size (B) of changes in temperature (T) and oxygen pressure can be described as $\Delta B/B \cdot 1/\Delta T = TSE + OSE$, where both the TSE and OSE can be related to species traits that govern the thermal and geometric dependence of O_2 supply and demand (see SM). The body size of fossil organisms can be used as a recorder of past changes in ocean P_{O_2}, provided that seawater temperature and physiological parameters that link body size to seawater P_{O_2} and temperature are known. Changes in T and B are measurable from the fossil record, whereas the allometric and thermal sensitivities of O_2 supply and demand have been obtained from comparative experimental respirometry on a large number of living organisms (*34*) (figs. S1 and S2 and table S3).

We used the model to estimate seawater P_{O_2} from published planktic and benthic foraminifera size data and the available sea-surface temperature (SST) estimates for the PETM from Pacific Sites 1209 and 1210 (*37*, *38*). Because global temperature rose by about 5°C at the onset of the PETM (Fig. 3D and fig. S8) (*17*), the expected response of foraminifera body size is to decrease according to the TSE. However, in Pacific Sites 1209 and 1210, planktic foraminifera that belong to genus *Morozovella*, which represents the dominant taxon of the PETM foraminifera assemblage in these Sites (*38*), collectively show a rise in body size at the onset of the PETM (Fig. 2C). Other taxa in the planktic foraminifera assemblage show a much more muted increase in size (fig. S7), but none of the planktic species show dwarfing (*38*). Our metabolic model indicates that the observed planktic foraminifera size changes (including the lack of dwarfing) in all dominant taxa correspond to an increase of subsurface FS-P_{O_2} in the tropics during the PETM (Fig. 3C and fig. S7). These results support a broader-scale rise in tropical shallow subsurface oxygen availability as the driver of the ODZ contraction indicated by our FB-$\delta^{15}N$ data. Benthic foraminifera from the same Sites show the opposite trend (Fig. 2D), implying that a reduction in P_{O_2} accompanied warming in the deep ocean (Fig. 3C).

Mechanisms of upper-ocean oxygenation in a warming climate

In the context of a warming ocean, a rise in subsurface O_2 requires a decline in respiratory O_2 consumption at depth relative to the rate of circulation-driven gross O_2 supply. A reduction in respiration during the PETM would require a decrease in export production, driven by reduced nutrient supply to the equatorial and eastern tropical Pacific surface waters (*6*, *39*). A decline in nutrient supply may be linked to a reduction either in tropical upwelling (*6*) or

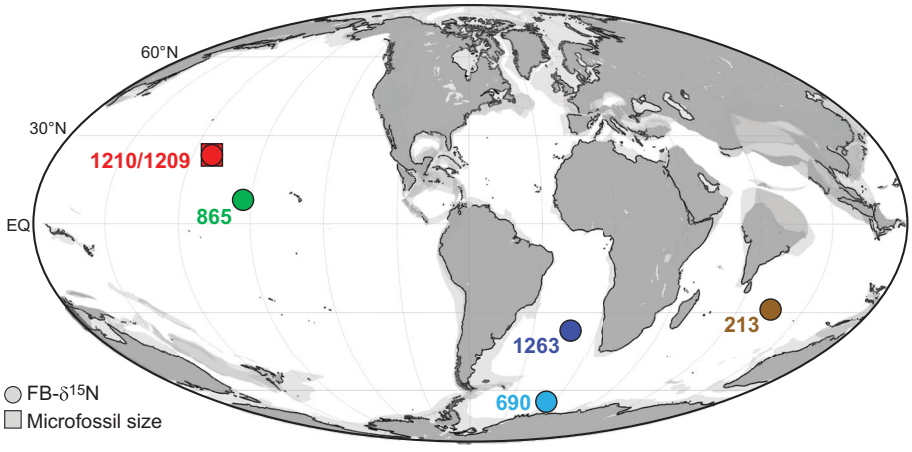

Fig. 1. Locations of sediments deposited during the PETM that were investigated in this study. Map showing a reconstructed paleogeography according to a plate rotation model (see SM) at 55.8 million years ago (PETM). All numbers refer to the DSDP or ODP Site identifier. Site locations are moved consistently with the same plate model. Circles and squares indicate site locations for FB-$\delta^{15}N$ measurement and FS-P_{O_2} reconstruction, respectively. EQ, equator.

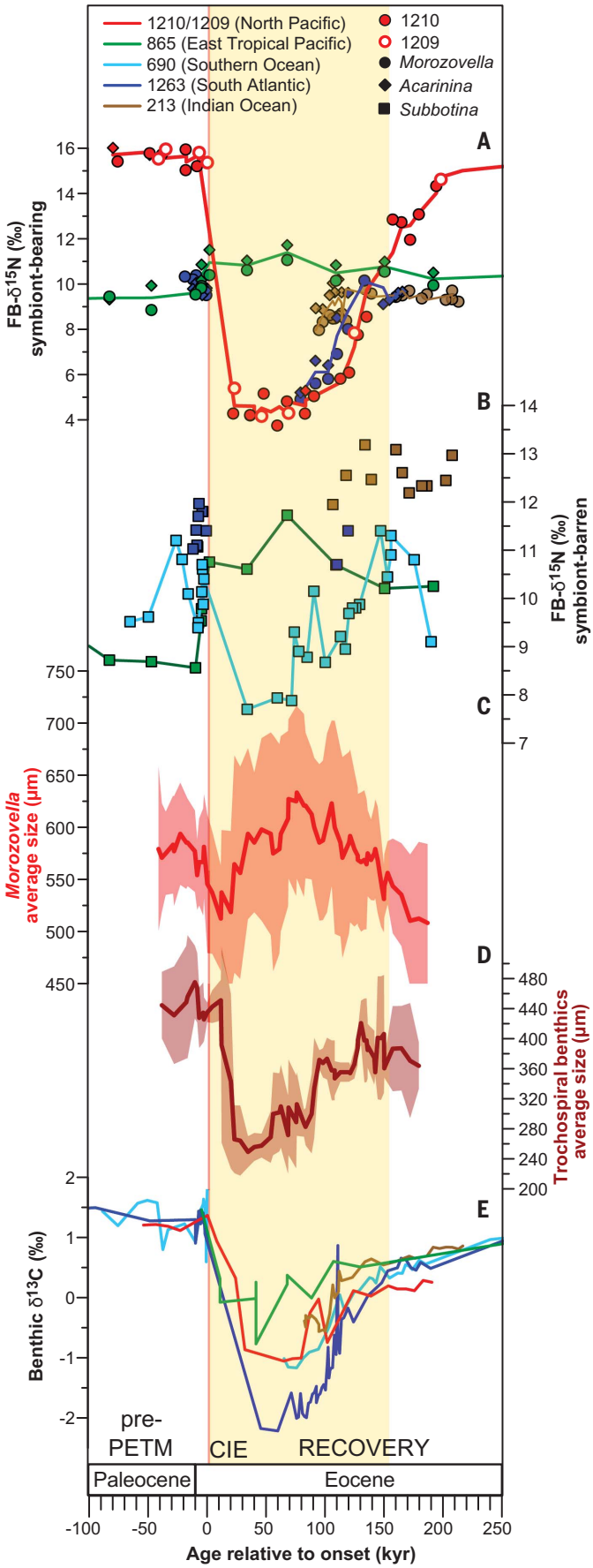

Fig. 2. FB-δ^{15}N and foraminifera shell size changes during the PETM. (**A**) FB-δ^{15}N of symbiont-bearing planktic foraminifera *Acarinina* (diamonds) and *Morozovella* (circles). (**B**) FB-δ^{15}N of symbiont-barren planktic foraminifera (*Subbotina*). FB-δ^{15}N measurement precision is ~0.2‰ (1 SD). (**C**) Shell size of planktic foraminifera of *Morozovella* spp. for Sites 1209 and 1210, using data from (*38*). The red line is a three-point interspecies moving average for both sites, and shading represents a 1-SD envelope. The dataset used for this figure and additional data from other planktic foraminifera in these sites are discussed in the SM. (**D**) Size of trochospiral benthic foraminifera for Sites 1209 and 1210, using data from (*37*). The brown line is a three-point moving average for both sites, and shading represents a 1-SD envelope. (**E**) Carbonate δ^{13}C records from benthic foraminifera *Nuttallides truempyi* or *Cibicidoides* spp. δ^{13}C, indicating the CIE, which is a common marker of the PETM (see SM for source data). In all panels but (D), color reflects the relevant DSDP or ODP Site (see the legend). The vertical light red line indicates the onset of the PETM; the yellow shading indicates the approximate duration of the event (~150 thousand years (kyr).

in the nutrient concentration of the upwelled waters. The former is controlled mainly by tropical trade winds, whereas the latter is controlled by the degree of nutrient consumption in the mid-latitude surface regions that ventilate the tropical thermocline (*8*, *40*). Such changes could have occurred even on a decadal-centennial timescale (*41*), consistent with the abruptness of the FB-δ^{15}N decline and FS-P_{O_2} rise, with a near-lack of intermediate values (Fig. 1A). Both of these mechanisms could have contributed to the O_2 changes that we observed. Changes in O_2 supply ("ventilation") by upper-ocean circulation cannot be ruled out. However, rapid warming intervals are typically associated with reduced rates of ventilation (*42*), which would tend to work against the observed PETM oxygenation, exacerbating the need for lower tropical productivity. With regard to nutrient concentration, there have been suggestions of a global increase in nutrient reservoir during the PETM (*43*); this alone would increase nutrient supply to tropical surface waters, the opposite of what is needed to explain the Site 865 data and the ODZ contraction.

The FB-δ^{15}N data from East Pacific Site 865 reported here support a decline in upwelling-fueled phytoplankton productivity as the most likely cause of ODZ contraction during the PETM. In contrast to all other records across the PETM, Site 865 shows a 2‰ rise in FB-δ^{15}N for both symbiont-bearing and symbiont-barren foraminifera (Fig. 2, A and B). The difference from nearby Site 1210 is stark: Before the PETM, Site 865 shows FB-δ^{15}N values 6‰ lower than those of Site 1210, whereas at the CIE onset, FB-δ^{15}N at Site 865 is 6‰ higher than FB-δ^{15}N at Sites 1209 and 1210 (Fig. 2, A and B, and fig. S6). During the PETM, Site 865 was located within 6° of latitude from the equator (Fig. 1 and table S1). In the modern ocean, the equatorial Pacific hosts high rates of primary production associated with intense equatorial upwelling, with a large "nutrient tongue" in these surface waters, where the isotopic discrimination associated with partial nitrate assimilation leads to a low FB-δ^{15}N (*44*). Similar conditions during the Paleogene are supported by both geological evidence of high equatorial sedimentation rates (*45*) and the low FB-δ^{15}N of Site 865 relative to that of Site 1210 at that time (Fig. 2A). The net rise in FB-δ^{15}N at Site 865 (Fig. 3A) and the reversal of the FB-δ^{15}N difference between Sites 865 and 1210 at the CIE onset (fig. S6) are best explained by an increase in the degree of nutrient consumption in the equatorial upwelling zone and a contraction of the nutrient tongue during the PETM. Studies of nannofossil assemblages at Site 865 have been interpreted to reflect a shift from eutrophic toward oligotrophic conditions at the onset of the CIE (Fig. 3A) (*46*), which supports this interpretation of the Site 865 FB-δ^{15}N record. A decrease in either the tropical

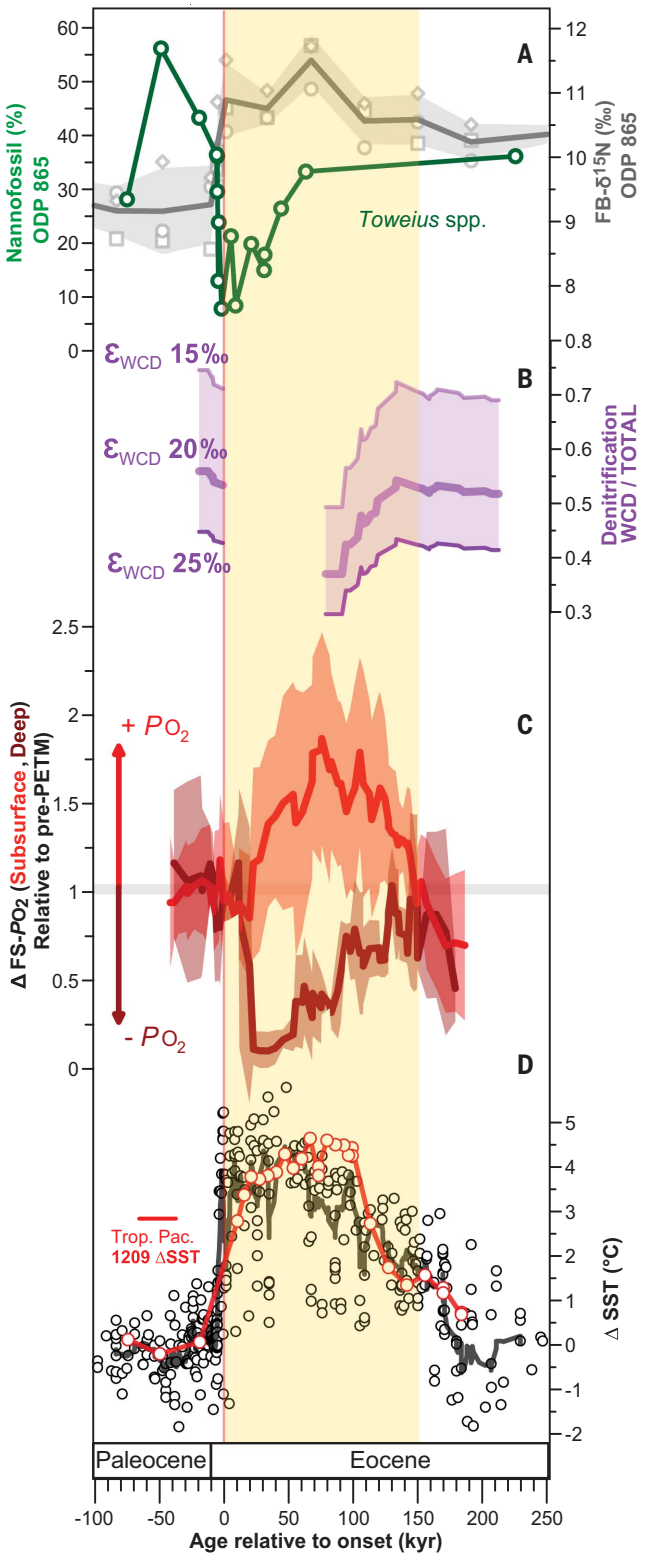

Fig. 3. Comparison of near-equatorial FB-δ^{15}N data with reconstructions of low-latitude stratification, global ocean denitrification change, and shallow and deep oxygen change. (**A**) FB-δ^{15}N change in near-equatorial Pacific Site 865 in three different planktic foraminifera taxa: *Morozovella* (circles), *Acarinina* (diamonds), and *Subbotina* (squares). Relative abundance of coccolithophore *Toweius* spp. from (*46*), which dwell in eutrophic conditions, suggesting a decline in nutrient supply at the PETM. Shading represents 1 SD of the mean of the three foraminifera taxa. (**B**) Estimated changes in the ratio of WCD to total denitrification, based on an isotope budget constructed from Sites 1263 and 213 FB-δ^{15}N data. Shading represents the plausible range of values using three different denitrification isotopic fractionation factors (ε_{WCD}). (**C**) Time series of estimated changes in subsurface (red) and deep ocean(brown) FS-P_{O_2} relative to pre-PETM using the metabolic model applied to foraminifera size in tropical Pacific Sites 1209 and 1210. Red and brown lines are three-point moving averages, and shading represents a 1-SD envelope. (**D**) Compilation of planktic foraminifera Mg/Ca- and lipid biomarker (TEX_{86})–based upper-ocean temperature changes, plotted relative to pre-PETM average values. The black line is a nine-point moving average. The red line represents the upper-ocean temperature reconstruction used for shallow subsurface P_{O_2} estimation in Sites 1209 and 1210 (see SM for source data). The vertical light red line indicates the onset of the PETM; the yellow shading indicates the approximate duration of the event (~150 kyr).

upwelling rate or the nutrient concentration of the upwelling waters could have caused the contraction in the equatorial Pacific nutrient tongue and the decline in tropical productivity.

The foraminifera body-size changes during the PETM that are observed at Sites 1209 and 1210 also support an upper-ocean mechanism for the oxygenation of the tropical Pacific thermocline. Although the body size of planktic foraminifera did not decrease, contrary to expectations from the TSE, that of benthic foraminifera decreased by ~20% per °C, far more than can be attributed to temperature alone. This implies that the P_{O_2} of waters at ~2000 m decreased while temperatures rose (Fig. 4A). A rise in deep Pacific O_2 and its mixing into the thermocline was therefore not the cause of the PETM increase in O_2 in the tropical shallow subsurface. Warming without a change in the respiratory O_2 consumption will cause a reduction in P_{O_2} owing to the nonlinear thermal solubility of gases, but this effect is small. Thus, the apparent decline in abyssal P_{O_2} implies a reduction of surface nutrients in the polar or subpolar regions ventilating the ocean's interior (*47*). This may have contributed to the loss of productivity in the tropics and the resulting rise of tropical shallow subsurface O_2, a mechanism previously seen in models of past and future global warming (*8*, *48*).

Comparison of reconstructed oxygen changes to numerical simulations

We compared the magnitude and pattern of P_{O_2} changes inferred from foraminifera body size to those of numerical experiments conducted with an ocean general circulation model (Fig. 4; see SM). The model is forced with SST from proxy reconstructions across the PETM (*17*), and circulation changes are imposed from a coupled climate model (*42*). The model reproduces deep ocean temperatures in the pre-PETM and peak-PETM (fig. S9), for which it also simulates the equilibrium distributions of O_2 and nutrients. Across a range of simulations that vary the magnitude of circulation change and the depletion of surface nutrients (fig. S10), the P_{O_2} rises in the low-latitude thermocline while declining in the high latitudes and the deep ocean (Fig. 4A). These changes are consistent in magnitude and pattern with the changes in P_{O_2} reconstructed from both planktic and benthic foraminifera body size (Fig. 3C).

The observed oxygenation of the tropical thermocline and the ODZ contraction during the PETM may be relevant for the coming decades and centuries. This suggestion is supported by the strong agreement in the rate of tropical P_{O_2} change per °C of warming of our reconstructions with PETM model simulations (Fig. 4A) and with future climate projections for the year 2300 under a high–greenhouse gas emissions scenario [Fig. 4B; (*48*)]. The inferred contraction of the equatorial nutrient tongue during the PETM is likewise consistent with Earth System Model simulations of future global warming, which suggest a decrease in primary production and nutrient concentrations by the end of this century (*49*, *50*). Thus, our PETM results support the expectation that the ODZs of the ocean will likely contract in response to global warming

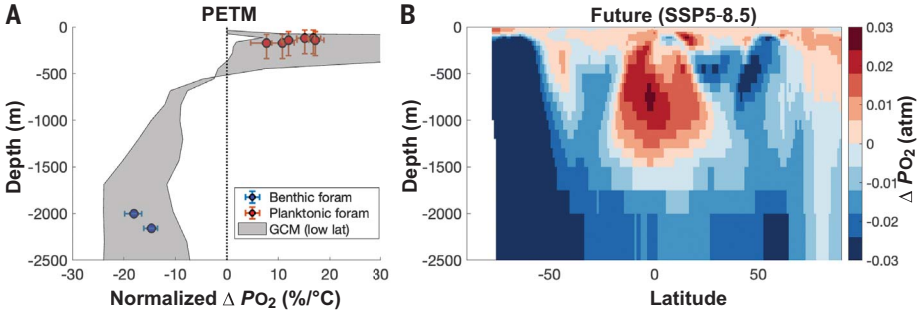

Fig. 4. Change in ocean P_{O_2} from past and future climate warming. (**A**) Vertical profile of percentage P_{O_2} change per °C of warming, estimated from the metabolic model applied to body-size and temperature proxy records from foraminifera (foram) in the tropical Pacific. The shaded curve is the range of low-latitude Pacific P_{O_2} change from an ocean general circulation model (GCM), which simulates the rapid warming at the PETM for a range of scenarios for the biological carbon pump efficiency (see SM). (**B**) Meridional depth section of zonally averaged P_{O_2} change (atm) from Earth System Model projections of future warming in the year 2300 CE for the Shared Socioeconomic Pathway SSP5-8.5 scenario (see SM), which yield a similar vertical structure to projections from models of the PETM.

as a consequence of a reduction in productivity-driven oxygen demand in the surface tropical Pacific.

Implications for marine biodiversity

Our results have implications for marine life under abrupt climate warming. In the modern climate, the general increase in biodiversity from the poles toward the equator exhibits a reversal in the tropics (*51*), where the prevailing combination of high temperature and low O_2 is inhabitable for a smaller number of species (*52*). A warming climate pushes ocean temperatures beyond the metabolic limits of a greater number of species, further accentuating the tropical dip in species richness, a feature that arose after the Last Glacial Maximum (*53*). Unlike with the deglacial warmings of the Pleistocene, the rise in tropical O_2 reconstructed for the PETM would have maintained an aerobic habitat that would otherwise have been lost because of thermal acceleration of animal metabolism. This compensation may help to explain the relatively moderate level of pelagic extinction in the fossil record of the PETM (*54*, *55*). By contrast, increased tropical subsurface O_2 change was not adequate to ward off massive losses of tropical biodiversity at the end-Permian (*48*) nor is it predicted to be in future projections of human-driven global warming (*52*).

REFERENCES AND NOTES

1. S. Schmidtko, L. Stramma, M. Visbeck, *Nature* **542**, 335–339 (2017).
2. T. Ito, S. Minobe, M. C. Long, C. Deutsch, *Geophys. Res. Lett.* **44**, 4214–4223 (2017).
3. L. Stramma, G. C. Johnson, J. Sprintall, V. Mohrholz, *Science* **320**, 655–658 (2008).
4. D. Breitburg *et al.*, *Science* **359**, eaam7240 (2018).
5. H.-O. Pörtner *et al.*, Eds., *Climate Change 2022: Impacts, Adaptation and Vulnerability: Working Group II Contribution to the Sixth Assessment Report of the Intergovernmental Panel on Climate Change* (Cambridge Univ. Press, 2023).
6. C. Deutsch *et al.*, *Science* **345**, 665–668 (2014).
7. A. Yamamoto *et al.*, *Global Biogeochem. Cycles* **29**, 1801–1815 (2015).
8. W. Fu, F. Primeau, J. K. Moore, K. Lindsay, J. T. Randerson, *Global Biogeochem. Cycles* **32**, 551–564 (2018).
9. E. R. Kast *et al.*, *Science* **364**, 386–389 (2019).
10. A. Auderset *et al.*, *Nature* **609**, 77–82 (2022).
11. X. T. Wang *et al.*, *Proc. Natl. Acad. Sci. U.S.A.* **119**, e2204986119 (2022).
12. R. S. Ganeshram, T. F. Pedersen, S. E. Calvert, J. W. Murray, *Nature* **376**, 755–758 (1995).
13. A. S. Studer *et al.*, *Paleoceanogr. Paleoclimatol.* **36**, e2020PA004063 (2021).
14. J. Zachos, M. Pagani, L. Sloan, E. Thomas, K. Billups, *Science* **292**, 686–693 (2001).
15. S. Kirtland Turner, P. M. Hull, L. R. Kump, A. Ridgwell, *Nat. Commun.* **8**, 353 (2017).
16. F. A. McInerney, S. L. Wing, *Annu. Rev. Earth Planet. Sci.* **39**, 489–516 (2011).
17. J. E. Tierney *et al.*, *Proc. Natl. Acad. Sci. U.S.A.* **119**, e2205326119 (2022).
18. R. E. Zeebe, J. C. Zachos, G. R. Dickens, *Nat. Geosci.* **2**, 576–580 (2009).
19. D. E. Penman, B. Hönisch, R. E. Zeebe, E. Thomas, J. C. Zachos, *Paleoceanography* **29**, 357–369 (2014).
20. E. Thomas, N. J. Shackleton, *Spec. Publ. Geol. Soc. London* **101**, 401–441 (1996).
21. R. E. Zeebe, A. Ridgwell, J. C. Zachos, *Nat. Geosci.* **9**, 325–329 (2016).
22. W. Yao, A. Paytan, U. G. Wortmann, *Science* **361**, 804–806 (2018).
23. X. Zhou, E. Thomas, R. E. M. Rickaby, A. M. E. Winguth, Z. Lu, *Paleoceanography* **29**, 964–975 (2014).
24. M. A. Altabet, R. Francois, D. W. Murray, W. L. Prell, *Nature* **373**, 506–509 (1995).
25. J. D. Cline, I. R. Kaplan, *Mar. Chem.* **3**, 271–299 (1975).
26. D. M. Sigman, P. J. DiFiore, M. P. Hain, C. Deutsch, D. M. Karl, *Geophys. Res. Lett.* **36**, 2008GL035784 (2009).
27. J. A. Brandes, A. H. Devol, *Geochim. Cosmochim. Acta* **61**, 1793–1801 (1997).
28. J. A. Brandes, A. H. Devol, *Global Biogeochem. Cycles* **16**, 67-1–67-14 (2002).
29. H. Ren, D. M. Sigman, R. C. Thunell, M. G. Prokopenko, *Limnol. Oceanogr.* **57**, 1011–1024 (2012).
30. A. Martínez-García *et al.*, *Geochem. Geophys. Geosyst.* **23**, e2022GC010396 (2022).
31. D. Bianchi, J. P. Dunne, J. L. Sarmiento, E. D. Galbraith, *Global Biogeochem. Cycles* **26**, 2011GB004209 (2012).
32. F. Fripiat *et al.*, *Nat. Geosci.* **14**, 855–861 (2021).
33. D. Atkinson, *Adv. Ecol. Res.* **25**, 1–58 (1994).
34. C. Deutsch *et al.*, *Proc. Natl. Acad. Sci. U.S.A.* **119**, e2201345119 (2022).
35. M. Czarnoleski, J. Ejsmont-Karabin, M. J. Angilletta Jr., J. Kozlowski, *Ecosphere* **6**, art164 (2015).
36. A. Kuroyanagi *et al.*, *Mar. Micropaleontol.* **101**, 28–32 (2013).
37. K. Kaiho, K. Takeda, M. R. Petrizzo, J. C. Zachos, *Palaeogeogr. Palaeoclimatol. Palaeoecol.* **237**, 456–464 (2006).
38. M. R. Petrizzo, *Mar. Micropaleontol.* **63**, 187–200 (2007).
39. J. J. M. Busecke, L. Resplandy, S. J. Ditkovsky, J. G. John, *AGU Adv.* **3**, e2021AV000470 (2022).
40. D. P. Keller, I. Kriest, W. Koeve, A. Oschlies, *Geophys. Res. Lett.* **43**, 6469–6477 (2016).
41. S. Yang, N. Gruber, M. C. Long, M. Vogt, *Global Biogeochem. Cycles* **31**, 1470–1487 (2017).
42. T. Ilyina, M. Heinze, *Geophys. Res. Lett.* **46**, 842–852 (2019).
43. N. M. Papadomanolaki, W. K. Lenstra, M. Wolthers, C. P. Slomp, *Sci. Adv.* **8**, eabn2370 (2022).
44. P. A. Rafter, D. M. Sigman, K. R. M. Mackey, *Nat. Commun.* **8**, 1100 (2017).
45. T. C. Moore Jr. *et al.*, *Paleoceanography* **19**, 2003PA000998 (2004).
46. D. Clay Kelly, T. J. Bralower, J. C. Zachos, I. P. Silva, E. Thomas, *Geology* **24**, 423 (1996).
47. J. L. Sarmiento, J. R. Toggweiler, *Nature* **308**, 621–624 (1984).
48. J. L. Penn, C. Deutsch, J. L. Payne, E. A. Sperling, *Science* **362**, eaat1327 (2018).
49. Y. Takano, T. Ito, C. Deutsch, *Global Biogeochem. Cycles* **32**, 1329–1349 (2018).
50. L. Kwiatkowski *et al.*, *Biogeosciences* **17**, 3439–3470 (2020).
51. C. Chaudhary, H. Saeedi, M. J. Costello, *Trends Ecol. Evol.* **31**, 670–676 (2016).
52. J. L. Penn, C. Deutsch, *Science* **376**, 524–526 (2022).
53. M. Yasuhara *et al.*, *Proc. Natl. Acad. Sci. U.S.A.* **117**, 12891–12896 (2020).
54. R. D. Norris, S. K. Turner, P. M. Hull, A. Ridgwell, *Science* **341**, 492–498 (2013).
55. J. Frieling *et al.*, *Sci. Adv.* **3**, e1600891 (2017).
56. S. Moretti, Oxygen rise in the tropical upper ocean during the Paleocene-Eocene Thermal Maximum [Dataset]. Dryad (2023); https://doi.org/doi:10.5061/dryad.brv15dvdr.

ACKNOWLEDGMENTS

We thank two anonymous reviewers for their comments and suggestions. We thank M. Schmitt, F. Rubach, and B. Hinnenberg for assistance in the laboratory and S. Oleynik for advice on instrumentation. **Funding:** This work was funded by the Max Planck Society (MPG). V.L. and R.D. were supported by MIUR P.R.I.N. 2017 grant (2017RX9XXXY). C.D. was supported by the National Science Foundation (EAR-2121466). D.M.S. received support from the Tuttle Fund of the Department of Geosciences at Princeton University. **Author contributions:** S.M. and A.M.-G. designed the study. S.M. measured foraminifera-bound nitrogen isotopes in the lab of A.M.-G. C.D. developed the metabolic P_{O_2} model. S.M., A.M.-G., and D.M.S. wrote the first draft of the manuscript. Ro.S. and L.G. contributed to sample preparation under the supervision of Ra.S. E.T. provided sample material for Sites 1263 and 690. A.T. provided material for Site 865. M.R.P. provided material for Sites 1209 and 1210. Conceptualization: S.M., C.D., D.M.S., A.M.-G.; Methodology: S.M., C.D., Ro.S., L.G., D.M.S., A.M.-G.; Investigation: S.M., C.D.; Visualization: S.M., C.D., A.M.-G.; Resources: A.A., E.T., R.N., A.T., P.S., V.L., M.R.P., Ra.S., R.D., G.H.H., A.M.-G.; Funding acquisition: C.D., V.L., R.D., G.H.H., A.M.-G.; Project administration: A.M.-G.; Supervision: D.M.S., A.M.-G.; Writing – original draft: S.M., D.M.S., A.M.-G.; Writing – review and editing: All authors. **Competing interests:** The authors declare that they have no competing interests. **Data and materials availability:** Datasets are available as data S1 and S2 and at Dryad (*56*).

SUPPLEMENTARY MATERIALS

science.org/doi/10.1126/science.adh4893
Materials and Methods
Supplementary Text
Figs. S1 to S10
Tables S1 to S5
References (*57*–*108*)
Data S1 and S2

Submitted 2 April 2023; accepted 14 January 2024
10.1126/science.adh4893